JOURNAL OF Materials CHEMISTRY

New rare-earth (Y, Yb) bismuth(III) germanates. An initial study of a promising series†

Concepción Cascales,*[a] Juan Antonio Campa,[b] Enrique Gutiérrez Puebla,[a] M. Angeles Monge,[a] Caridad Ruíz Valero[a] and Isidoro Rasines[a]

[a]*Instituto de Ciencia de Materiales de Madrid, Consejo Superior de Investigaciones Científicas, Cantoblanco, E-28049 Madrid, Spain. E-mail: ccascales@icmm.csic.es; Fax: +34 91 372 0623*
[b]*Facultad de Ciencias, Universidad Complutense de Madrid, Madrid E-28040, Spain*

Received 5th August 2002, Accepted 6th August 2002
First published as an Advance Article on the web 9th September 2002

Colored crystals of the middle term ($a = 1$) of the $Bi_{2-a}R_aGeO_5$ series (R = Y (yellow), Yb (brown)) have been grown. The structure of these materials has been established by single-crystal X-ray diffraction. They are isostructural and crystallize in the orthorhombic system, space group *Pbca* (No. 61), $Z = 8$, with unit-cell parameters $a = 5.341(8)$ and $5.315(2)$, $b = 15.232(2)$ and $15.225(2)$, $c = 11.084(3)$ and $11.025(2)$ Å, for R = Y and Yb respectively. The structure is formed by $[GeRO_5]_\infty$ layers containing both $(RO_7)_6$ units and GeO_4 tetrahedra. Between these layers zig-zag chains of ψ-BiO_5 octahedra run in the *a* direction. The stereoelectronic effect of the Bi^{3+} lone pair leads to this apparent zig-zag, and therefore to the kind of packing observed in this new type of structure. The downward deviation in the molar magnetic susceptibility of $BiYbGeO_5$ from the Curie–Weiss behavior, observed at low temperatures, is attributed to the effect of the crystal field splitting of the $^2F_{7/2}$ ground term of Yb^{3+}. Energies of the maximum phonon, 799 and 797 cm^{-1} for Y and Yb materials, respectively, have been determined from room temperature Raman scattering spectra of polycrystalline samples.

Introduction

Although the germanates R_2GeO_5, R = rare-earth, and Bi_2GeO_5 were studied[1–6] years ago, the possible compounds of the $Bi_{2-a}R_aGeO_5$ ($0 < a < 2$) series are presently unkonwn. However, it is likely that the simultaneous presence of Bi^{3+}, which possesses a non-bonding $6s^2$ electron pair, and trivalent R in these compounds leads to interesting physical properties.

In some of the published work concerning Bi^{3+} materials the presence of the lone pair has not even been mentioned, *e.g.* for the scheelite-type $(Eu_{0.28}Bi_{0.72})VO_4$ studied for Eu^{3+} luminescence,[7] or in $(R_aBi_{2a})O_3$ (R = Gd, Pr, Sm, Eu, Gd, Tb, Dy) materials.[8–11] In contrast, the low solid-state intersolubility of isostructural rare-earth laser hosts $NaBi(XO_4)_2$ and $NaR(XO_4)_2$, X = Mo and W, has been explained on the basis of the very different electron structure of Bi^{3+} and R^{3+},[12] which, however, have very similar ionic radii. Similarly, the limited substitution of Bi^{3+} by R^{3+} ions found in optoelectronic or scintillator $Bi_{12}SiO_{20}$ and $Bi_4Ge_3O_{12}$ materials, respectively,[13] may be attributed to the large electronegativity of Bi^{3+}.[12] The lone $6s^2$ electron pair also provides the great structural flexibility of the sillenite structure of $Bi_{12}SiO_{20}$, allowing change not only of the geometry of the coordination environment of Bi^{3+}, but even of the coordination itself, and consequently results in the appearance of several different optically active sites that show individual optical properties when it is replaced by Nd or Eu.[14]

By taking into account the feasible statistical inter-replacement of Bi^{3+} and R^{3+},[12–15] $Bi_{2-a}R_aGeO_5$ phases could be partially disordered hosts for lasing rare-earth ions. This disorder is claimed to be the origin of the spectral line broadening in optical absorption and photoluminescence, even at low temperatures,[16–19] which allows significant practical applications in laser devices,[20,21] like laser tunability, improved efficiency for absorption of diode pumping[22] or suitability for hole burning optical memories.[23] Moreover interesting phenomena related to room temperature laser line narrowing can occur, which are associated with the migration of energy among the coexisting optical centers.[20]

On the other hand, the search for new R-doped hosts with maximum phonon energies lower than those of silica is very worthy as they will provide the possibility of developing higher performance laser and fiber optics amplifiers. Low phonon energies are required to reduce the non-radiative multiphonon relaxation rates of the excited states of R ions, which results in increased lifetimes of some excited levels and consequently in the enhanced quantum efficiency of the luminescence. Moreover this property can positively affect up-conversion pumping schemes, allowing the creation of visible crystalline lasers with infrared laser diode excitation.[24]

To our knowledge there have been no reports on germanate compounds containing similar amounts of Bi and a rare-earth metal. Here we study what happens around the middle of the proposed $Bi_{2-a}R_aGeO_5$ series, and in this case whether the structure of either of the limiting phases Bi_2GeO_5 ($a = 0$) and R_2GeO_5 ($a = 2$) is maintained or collapses to give a different type of structure. Y and Yb were the rare-earths selected since they are similar sizes, and so compounds containing these rare-earth metals will possibly adopt the same crystal structure. However, Y^{3+} is diamagnetic and the $4f^{13}$ Yb^{3+} cation is paramagnetic.

In this paper, which signifies a first step in what could be interesting research into a new type of material, we report the existence of germanates that are middle terms in the $Bi_{2-a}R_aGeO_5$ series, R = Y, Yb. We also report how single crystals of these compounds were grown, their novel structure type established by single crystal X-ray diffraction techniques, and the stereochemical role of the Bi^{3+} lone pairs. The X-ray powder diffraction pattern for R = Yb is now available.

†Electronic supplementary information (ESI) available: table containing observed and calculated 2θ, observed d-spacings and intensities of each *hkl* peak for $BiYbGeO_5$. See http://www.rsc.org/suppdata/jm/b2/b207638c/

 DOI: 10.1039/b207638c

Results of the magnetization measurements for R = Yb are presented. Finally, the highest phonon energy of the crystal host is determined from room temperature Raman spectra of polycrystalline samples of both Y and Yb materials.

Experimental

Colored single crystals corresponding to the formula $BiRGeO_5$ (R = Y or Yb) were found (R = Y, yellow; R = Yb, brown) in products resulting from the following procedure. Reagent grade Bi_2O_3, R_2O_3 and GeO_2 were intimately mixed in the molar ratios 8 : 1 : 4, respectively, and heated to 1050 °C using platinum crucibles and an electric furnace. After soaking for 1 h, the melt was cooled to 800 °C at a rate of 4 °C h^{-1}, and subsequently cooled to room temperature after turning the power off. The excess of flux was completely removed with dilute nitric acid, and the crystals were filtered off, washed with distilled water, and dried at ambient temperature.

Polycrystalline samples of $BiRGeO_5$ (R = Y, Yb) were prepared in platinum crucibles from mixtures of reagent grade Bi_2O_3, R_2O_3 and GeO_2 in molar ratios of 1 : 1 : 2, respectively. The mixtures were ground, heated in air at successive temperatures (°C) of 800, 900 and twice at 950, quenched and reground after each of these stages that lasted 1 day.

The structure of $BiRGeO_5$ (R = Y, Yb) was determined by single-crystal X-ray diffraction methods. Two crystals (R = Y, Yb) with prismatic morphology were mounted in an Enraf-Nonius CAD-4 diffractometer in which graphite-monochromated Mo-Kα radiation, $\lambda = 0.71069$ Å, was employed. The cell dimensions were refined by least-squares fitting of the 2θ values of 25 reflections, resulting in orthorhombic lattice parameters. Both compounds are isostructural. A summary of the fundamental crystal and refinement data are given in Table 1. The systematic absences $k = 2n + 1$ for $0kl$, $l = 2n + 1$ for $h0l$ and $h = 2n + 1$ for $hk0$ were consistent with the space group *Pbca*. Intensity data were collected using the $\omega/2\theta$ scan mode with standard reflections monitored for intensity changes throughout the data collection. The reflections were corrected for Lorentz and polarization effects. Scattering factors for neutral atoms and anomalous dispersion corrections for Bi, Yb, Y and Ge were taken from *International Tables for X-Ray Crystallography*.[25] The structure was solved by Patterson and Fourier methods. The Bi and R (Y or Yb) atoms are situated at different positions. In the compound where R = Y the isotropic thermal parameter for Y became negative and it was necessary to refine the occupancy factor (o.f.) for this atom. The site is preferentially occupied by Y (o.f. = 0.88) but there is 0.12 of extra Bi. With the refinement of the occupancy factor for the Y atom, the isotropic thermal parameter changed to a normal and positive value, and the *R* value was lower. Partial substitution was not observed in the case of R = Yb. An empirical absorption correction was applied at the end of the isotropic refinement.[26] For $BiYGeO_5$ anisotropic full matrix least-squares refinement with unit weights led to $R = 0.039$ and $R_w = 0.046$, and no trend in F *vs.* F_o or $\sin\theta/\lambda$ was observed. The last steps of the refinement for $BiYbGeO_5$ were calculated by PESOS[27] with weights $w = w_1w_2$, where $w_1 = 1/(a + b|F_o|)^2$ and $w_2 = 1/(c + d(\sin\theta/\lambda))$, with the following coefficients for $|F_o| < 101$, $a = 24.6$, $b = -0.16$, and for $101 < |Fo| < 1200$, $a = 4.5$, $b = 0.01$. A final difference synthesis showed no significant electron density. Most of the calculations were carried out with the X-ray 80 System.[28]

CCDC reference numbers 179846 and 179847.

See http://www.rsc.org/suppdata/jm/b2/b207638c/ for crystallographic files in CIF or other electronic format.

Standard X-ray powder diffraction (XRPD) analysis of polycrystalline samples was performed to test the crystal structure of these materials. The samples appeared to be well crystallized and completely free of other phases. The XRPD pattern for the intensity determination of observed reflections in $BiYbGeO_5$ was measured using a Siemens Kristalloflex 810 generator, Cu-Kα radiation ($\lambda = 1.540598$ Å) and a computer-controlled D-500 goniometer equipped with a graphite monochromator. The data were collected at room temperature over an angular range of $5° \leqslant 2\theta \leqslant 130°$, and were analyzed by the Rietveld profile analysis method using the WinPLOTR program.[29] Starting values of the unit cell and positional parameters used in the refinement were those previously obtained in the single-crystal X-ray determination. Independently, d-spacing measurements were made at a scanning rate of 0.1° 2θ min^{-1}, using wolfram, $a = 3.16524(4)$ Å, as an internal standard

A SQUID magnetometer (Quantum Design) operating from 1.7 K to 300 K at 1000 Oe was used to perform the d.c. magnetization measurements. Diamagnetic corrections[30] for the magnetic susceptibility were taken into account in each case.

Raman spectra from polycrystalline powders were obtained with a Reninshaw Ramascope 2000 equipped with a CCD detector. The samples were excited with the 514.5 nm line of an Ar^+ laser. The spectra were recorded in the backscattering geometry at room temperature and corrected by the spectral response of the experimental set-up.

Table 1 Crystal and refinement data for $BiRGeO_5$

Formula	$BiYGeO_5$	$BiYbGeO_5$
Mol wt	450.5	653.5
Crystal system	Orthorhombic	Orthorhombic
Space group	*Pbca* (No. 61)	*Pbca* (No. 61)
Cell dimensions/Å		
a	5.341(8)	5.315(2)
b	15.232(2)	15.225(2)
c	11.084(3)	11.025(2)
Z	8	8
V/Å^3	901.9(3)	892.1(4)
D_{calcd}/g cm^{-3}	6.64	7.96
F(000)	1552	1800
T/K	295	295
μ(Mo-K$_\alpha$)/cm^{-1}	581.2	665.1
Crystal dimensions/mm^3	0.06 × 0.1 × 0.3	0.08 × 0.1 × 0.13
2θ range/°	2–60	2–60
Scan technique	$\omega/2\theta$	$\omega/2\theta$
Data collected	(0,0,0) to (7,21,15)	(0,0,0) to (7,21,15)
Unique data	1312	1267
Observed reflections	757	845
R_{int} (%)	0.4	0.5
Decay	—	—
Standard reflections	3/19	3/20
Weighting scheme	Unit	Unit
$R = \Sigma\|\Delta F\|/\Sigma\|F_o\|$	3.9	4
$R_w = (\Sigma w\|\Delta F\|^2/\Sigma w\|F_o\|^2)$	4.6	4.9
Maximum shift/error	0.002	0.02
Absorption correction range	0.95–1.06	0.86–1.42

Results and discussion

Final atomic positional and thermal isotropic parameters are listed in Table 2. The refinement of the occupancy factor of the Y site in the $BiYGeO_5$ crystal has shown the existence of some extra Bi atoms sharing this position with Y. Since this partial substitution is not detected either in the current single crystal X-ray analysis of $BiYbGeO_5$ or in polycrystalline isostructural R compounds,[31] it is likely that the excess of Bi atoms is present because of the method used to obtain the single crystals, that is, the large amount of Bi_2O_3 over the required stoichiometric quantity that is employed as the flux in the crystal growth.

Selected bond distances are provided in Table 3. From the XRPD pattern for $BiYbGeO_5$ (see supplementary information†), the obtained unit cell dimensions $a = 5.2965(9)$, $b = 15.206(2)$, $c = 10.942(2)$ Å, $V = 881.2(2)$ Å^3 are comparable to

Table 2 Atomic coordinates for $BiRGeO_5$ (R = Y, Yb)

Atom	*x*	*y*	*z*	U_{eq}/Å^{2a}	Occupancy factor
Bi1	0.9548(1)	0.23826(4)	0.14801(7)	30(3)	
Y	0.0055(3)	0.0525(1)	0.3595(2)	20(6)	0.88
Bi2	0.0055(3)	0.0525(1)	0.3595(2)	20(6)	0.12
Ge	0.0074(4)	0.4023(1)	0.4040(2)	20(5)	
O1	0.063 (3)	0.3014(9)	0.329(1)	40(30)	
O2	0.3056(3)	0.436(1)	0.457(1)	30(30)	
O3	0.319(3)	0.127(1)	0.474(1)	80(30)	
O4	0.249(3)	0.153(1)	0.236(1)	60(30)	
O5	0.363(3)	0.479(1)	0.189(1)	30(30)	
Bi	0.9566(1)	0.23775(4)	0.14698(7)	46(2)	
Yb	0.0083(1)	0.05292(5)	0.35952(7)	25(2)	
Ge	0.0063(4)	0.4030(1)	0.4031(2)	46(5)	
O1	0.066(3)	0.301(1)	0.329(1)	53(28)	
O2	0.303(3)	0.437(1)	0.458(2)	77(30)	
O3	0.314(3)	0.123(1)	0.474(1)	56(28)	
O4	0.252(3)	0.153(1)	0.236(1)	45(26)	
O5	0.351(3)	0.478(1)	0.192(1)	55(28)	

$^a U_{eq} = t(U_1U_2U_3)^{\ddagger} \times 10^4$

Table 3 Selected bond distances (Å) in $BiRGeO_5$

	Y	Yb
R–O2^1	2.30(2)	2.29(2)
R–O2^2	2.31(1)	2.31(2)
R–O3	2.38(2)	2.32(2)
R–O4	2.43(2)	2.42(2)
R–O4^3	2.31(2)	2.30(2)
R–O5^2	2.31(2)	2.29(2)
R–O5^4	2.32(2)	2.30(2)
Bi–O1^5	2.30(1)	2.30(1)
Bi–O1^6	2.32(2)	2.26(1)
Bi–O3^6	2.29(2)	2.30(1)
Bi–O4^5	2.26(2)	2.32(2)
Bi–O4^6	2.13(2)	2.13(2)
Ge–O1	1.77(1)	1.78(1)
Ge–O2	1.77(2)	1.77(2)
Ge–O3^1	1.74(2)	1.74(2)
Ge–O5^3	1.74(2)	1.76(2)

Symmetry code: ^{1} ($x-$, $-y$,1 $-z$); ^{2} ($-x$,$y-$,z); ^{3} ($x-$,y, $-z$); ^{4} ($-x$,$y-$, $-z$); ^{5} (1 + x,y,z); ^{6} (+ x,y, $-z$).

those found after the crystal structure refinement, $a = 5.315(2)$, $b = 15.225(2)$, $c = 11.025(2)$ Å, $V = 892.1(4)$ Å^3.

The germanate groups show the typical tetrahedral oxygen environment with distances and angles similar to those found[32–35] in other rare earth germanate compounds. The R (Y, Yb) atoms are seven-coordinated. Taking into account the geometrical criteria required for idealized polytype forms[36] as well as the results of our planarity study, we conclude that the shape of the RO_7 polyhedron is similar to the C_{2v}-monocapped trigonal prism. The RO_6 trigonal prism of Fig. 1 is capped by one O2^1 atom on the face defined by the O3–O4^3–O5^4–O2^2 atoms. The dihedral u_1 and u_2 angles indicate the planarity of two square faces, and u_3 corresponds to the capped face of the trigonal prism. These angles have values of 2.2°, 13.7° and 38.6°, close to those given in the literature[36] for the C_{2v} model of ideal ML_7 polyhedra, $u_1 = 0$, $u_2 = 0$, $u_3 = 41.5°$. Table 4 shows the main planes P defined for the YbO_7 polyhedron, as well as the results of the planarity study, where the values u_1, u_2 and u_3 are the corresponding supplementary angles ($180 - u$) to those mentioned above. The Bi coordination polyhedra are defined as ψ-octahedra to whose sixth vertex points the lone pair of Bi^{3+}.

The structure can be conceived as being formed by layers of $[GeRO_5]_\infty$ which contain $(RO_7)_6$ units of edge-sharing RO_7 polyhedra parallel to the *ac* plane, Fig. 2. The RO_7 polyhedra are joined through the O4–O5 edge in the *a* direction and through O2–O2^2 in the *c* direction. Isolated GeO_4 tetrahedra are joined to RO_7 through the O2 and O5 vertexes, and the layers are bent in the *c* direction as can be seen in Fig. 3. These layers are separated by Bi sheets, in which the Bi ψ-octahedra are joined to the GeO_4 tetrahedra through the O3 and O1 vertexes. These sheets consist of zig-zag chains of Bi polyhedra, which are joined through the O1–O4 edges and run parallel to the *a* direction, Fig. 4. The Bi^{3+} lone pair leads to this apparent zig-zag, introducing the stereoelectronic effect responsible for the packing in this new type of structure. Further, the above distribution of $[GeRO_5]_\infty$ layers and Bi ψ-octahedra sheets leads to a highly compact structure, as the calculated densities of the title compounds indicate, Table 1, and the small thermal anisotropic parameters found for the cations in their structure refinements correlate with this fact.

Coordination polyhedra of $BiRGeO_5$ (R = Y, Yb) can be compared with those established for M_2GeO_5 (M = R, Bi). As for the rare-earth coordination, the new $BiRGeO_5$ compounds

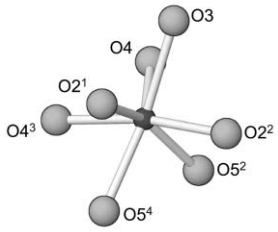

Fig. 1 RO_7 coordination polyhedron in $BiRGeO_5$ (R = Y, Yb). In order to define its shape, the calculated planes P for YbO_7 are given in Table 5.

Table 4 Planes P and principal angles (°) between them in theYbO_7 polyhedron

Planes	
P1 O3–O4–O4^3	P6 O2^2–O3–O5^2
P2 O2^2–O5^2–O5^4	P7 O3–O4–O5^2
P3 O2^2–O5^2–O4–O3	P8 O3–O4^3–O5^4
P4 O3–O4^3–O5^4–O2^2	P9 O3–O2^2–O5^4
P5 O2^1–O5^2–O5^4	
Principal angles/°	
P1–P2	4.9(6)
P2–P5 = u_3	141.4(6)
P6–P7 = u_1	177.8(6)
P8–P9 = u_2	166.3(6)

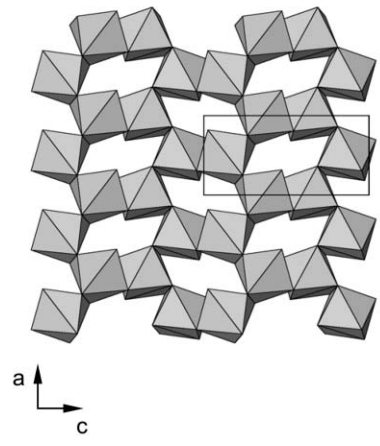

Fig. 2 View along the [010] direction of the $(RO_7)_6$ units in $[RGeO_5]_\infty$ layers .

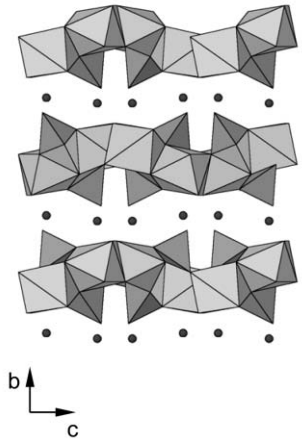

Fig. 3 View along the [100] direction of the lattice of $BiRGeO_5$ (R = Y, Yb). Small spheres represent Bi atoms.

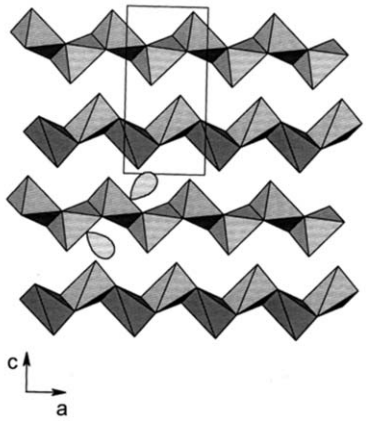

Fig. 4 View of the zig-zag Bi chains parallel to the *a* direction in $BiRGeO_5$ (R = Y, Yb). The lone pair is drawn for two ψ-BiO_5 octahedra.

contain only monocapped trigonal RO_7 prisms, whereas M_2GeO_5 (M = Nd, Eu, Gd, Dy) show monocapped trigonal MO_7 prisms together with NdO_8 cubes,[4] monocapped EuO_7 octahedra,[5] GdO_8 cubes,[5] and DyO_6 groups.[6] With regard to Bi, its coordination is different for each compound since it forms ψ-BiO_5 octahedra in $BiRGeO_5$, and trigonal BiO_6 prisms in Bi_2GeO_5.[1,2] Furthermore, the bond-valence[37] for Bi, which equals 3.2 for $BiRGeO_5$, reaches 2.6 for Bi_2GeO_5 when the six nearest oxygens are taken into account, and 2.7 when five additional and more distant oxygens are considered.

By comparing the unit cell parameters of the orthorhombic *Pbca* $BiRGeO_5$, $a = 5.315(2)$, $b = 15.225(2)$, $c = 11.025(2)$ Å (values for R = Yb) with those of the also orthorhombic $Cmc2_1$ Bi_2GeO_5, $a = 15.69(7)$, $b = 5.492(8)$, $c = 5.383(6)$ Å, it can be seen that the *c* axis of the former is twice the *b* axis of the latter, the other two being equal. Thus the formation of the $(RO_7)_6$ infinite layers in the new compounds forces the reorganization of the Bi and Ge polyhedra, doubling the unit cell. With Bi_2GeO_5 and R_2GeO_5 the two limits of the $Bi_{2-a}R_aGeO_5$ series, it can be concluded from the structural point of view for $a = 1.0$ that the new germanate structure is closer to Bi_2GeO_5. This makes sense since for *a* values close to 2 very different structure types appear in R_2GeO_5 depending on the size of R.

The temperature dependence of the molar d.c. magnetic susceptibility, χ_m, of $YbBiGeO_5$, and its reciprocal, are shown in Fig. 5. Above ~80 K the plot follows a Curie–Weiss type behaviour, $\chi^{-1} = [6.7(2) + 0.3744(9)T]$ mol emu^{-1} ($r = 0.9997$); the calculated magnetic moment, 4.6 μ_B, agrees very

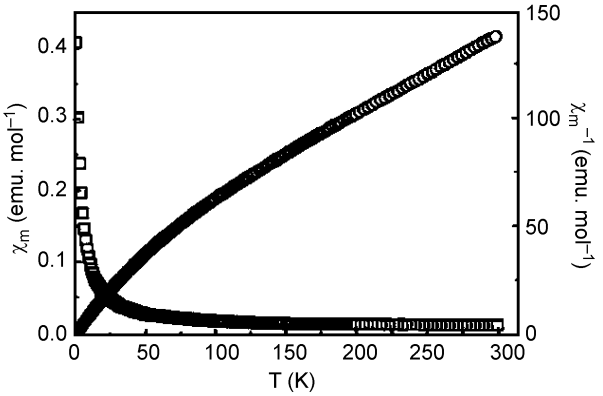

Fig. 5 Thermal variation of the molar dc magnetic susceptibility χ_m (squares), and its reciprocal (circles), for $BiYbGeO_5$.

well with the expected value, 4.5 μ_B, for the free-ion ground term $^2F_{7/2}$ of the Yb^{3+} ion. Since no maxima in χ_m are observed at low temperatures, it is clear that under 80 K the effect of the crystal-field splitting of this ground term is responsible for the downward deviation from linearity of the χ^{-1} *vs.* *T* plot. Often this deviation has been erroneously attributed to cooperative magnetic interactions, and in fact, it has been observed in other Yb compounds, for instance $Na_5Yb(MoO_4)_4$ (and also in $Na_5Yb(WO_4)_4$)[38] and $Yb_3Sb_5O_{12}$,[39] in which this kind of magnetic exchange is not present. Therefore, the Weiss constant for the material, $\theta_c = -71$ K, is entirely due to crystal-field effects.

The Raman spectra of polycrystalline samples of $BiYGeO_5$ and $BiYbGeO_5$ at room temperature are illustrated in Fig. 6. The similarity in the energies of all Raman peaks for both compounds is explained by the very small difference in Y and Yb ionic radii (0.035 Å), which induces very close interatomic distances in their networks. The energies of the maximum phonon are 799 and 797 cm^{-1} for Y and Yb compounds, respectively. These energies are somewhat lower than those observed (~930 cm^{-1})[40–43] for recently studied optically relevant crystal systems $M^IM^{III}(XO_4)_2$ (M^I = Li, Na, K;

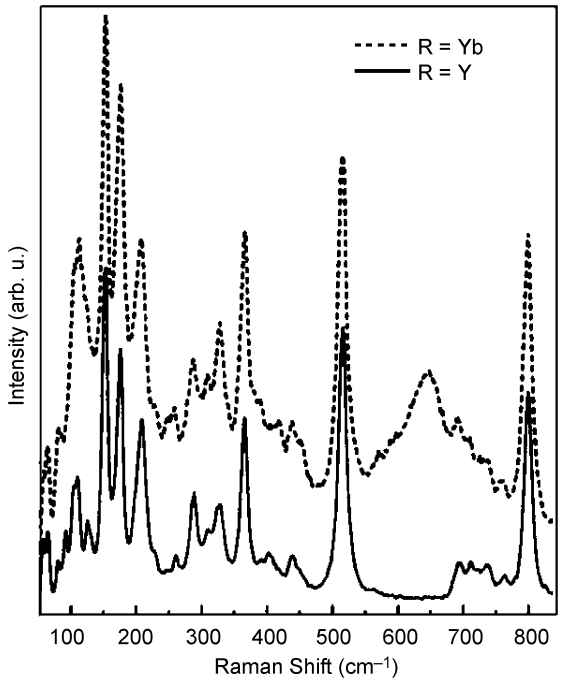

Fig. 6 Room temperature Raman spectra of polycrystalline $BiYGeO_5$ and $BiYbGeO_5$.

M^{III} = rare-earth; X = Mo, W). For crystal hosts with the above stoichiometry and M^{III} = Bi, the largest phonon energies are found to be $\sim$870–910 cm^{-1},[16,17,44,45] whereas for the polymorphic $CsBi(MoO_4)_2$ the largest phonon energy is $\sim$950 cm^{-1}.[46]

Conclusions

The existence of a new family of germanates of formula $BiRGeO_5$ (R = small rare-earth: Y, Yb) has been proved. The structure solved for single crystals of both Y and Yb phases is orthorhombic, space group *Pbca*. With regards to Bi_2GeO_5, *i.e.* the limiting phase with $a = 0$ of the $Bi_{2-a}R_aGeO_5$ series, the new packing appears to be a consequence of the formation of $(RO_7)_6$ units in the *ac* $[GeRO_5]_\infty$ layers, which forces the reorganization of Bi and Ge polyhedra doubling the initial unit-cell of Bi_2GeO_5. The zig-zag appearance of ψ-BiO_5 along *a* is induced by the stereoelectronic effect of the Bi^{3+} lone pair. Paramagnetic R containing compounds do not undergo any magnetic exchange interactions. Allowing for the possible partially disordered character of the matrix as well as for the energy of the largest phonon, which is lower than for other studied hosts, $BiRGeO_5$ seems to be a promising new crystal matrix for optically active dopants.

Acknowledgements

The authors acknowledge the financial support of Spanish DGESIC Projects PB97-1200, PB97-0246 and of the Unidad Asociada GBTYS of the University of Santiago de Compostela to the CSIC.

References

1 B. Aurivillius, C. I. Lindblom and P. Stenson, *Acta Chim. Scand.*, 1964, **18**, 1555.
2 A. Yu. Shaskov, V. A. Efremov, A. A. Bush, N. V. Rannev, Yu. N. Venevtsev and V. K. Trunov, *Zh. Neorg. Khim.*, 1986, **31**, 1391.
3 C. Sussieck-Fornefeld, *Heidelberg Geowiss. Abh.*, 1988, **17**, 139.
4 A. G. Vidgorchik, L. N. Dem'yanets and Yu. A. Malinovskii, *Kristallografiya*, 1987, **32**, 1381.
5 K. Kato, M. Sekita and K. Shigeyuki, *Acta Crystallogr., Sect. B*, 1979, **35**, 2201.
6 L. Brixner, J. Calabrese and H. Y. Chen, *J. Less-Common Met.*, 1985, **110**, 397.
7 J. L. Blin, A. Lorriaux-Rubens, F. Wallart and J. P. Wignacourt, *J. Mater. Chem.*, 1996, **6**, 385.
8 T. Yamamoto, R. Kanno, Y. Takeda, O. Yamamoto, Y. Kawamoto and M. Takano, *J. Solid State Chem.*, 1994, **109**, 372.
9 A. Watanabe, *J. Solid State Chem.*, 1995, **120**, 32.
10 Y. Jinling, L. Jingkui, T. Weihua, S. Ying, Ch. Xialong and R. Guanghui, *J. Solid State Chem.*, 1996, **125**, 85.
11 M. Drache, P. Conflant, S. Obbade, J. P. Wignacourt and A. J. Watanabe, *J. Solid State Chem.*, 1997, **129**, 98.
12 V. Volkov, M. Rico, A. Méndez Blas and C. Zaldo, *J. Phys. Chem. Solids*, 2002, **63**, 95.
13 A. A. Kaminskii, S. Sarkisov and G. Denisenko, *Phys. Status Solidi A*, 1984, **85**, 533.
14 C. Cascales, P. Porcher, J. Fernández, A. Oleaga, R. Balda and E. Diéguez, *J. Alloys Compd.*, 2001, **323-324**, 260.
15 L. N. Demaniets, A. N. Lobachev and G. A. Emelchenko, Rare-Earth Germanates, in *Crystals: Growth, Properties, and Applications*, vol. 4, ed. H. C. Freyhardt, Springer, Berlin, 1980, pp. 118–119.
16 J. Hanuza, A. Benzar, A. Haznar, M. Maczka, A. Pietraszko and J. H. van der Maas, *Vib. Spectrosc.*, 1996, **12**, 25.
17 J. Hanuza, A. Haznar, M. Maczka, A. Pietraszko, A. Lemiec, J. H. van der Maas and E. T. G. Lutz, *J. Raman Spectrosc.*, 1997, **28**, 953.
18 A. Méndez Blas, V. Volkov, C. Cascales and C. Zaldo, *J. Alloys Compd.*, 2001, **323-324**, 315.
19 M. Rico, V. Volkov, C. Cascales and C. Zaldo, *Chem. Phys.*, 2002, **279**, 73.
20 A. A. Kaminskii, *Phys. Status Solidi A*, 1995, **148**, 9.
21 A. A. Kaminskii, *Crystalline Lasers: Physical Processes and Operative Schemes*, CRC Press, Boca Raton, FL, 1996.
22 L. Fornasiero, T. Kellner, A. S. Kück, J. P. Meyn, P. E. A. Möbert and G. Hubert, *Appl. Phys B*, 1999, **68**, 67.
23 E. S. Manilof, A. E. Johnson and T. W. Mossberg, *MRS Bull.*, 1999, **24**, 46.
24 S. Tanabe, K. Suzuki, N. Soga and T. Hanada, *J. Opt. Soc. Am. B*, 1994, **11**, 933.
25 *International Tables for X-Ray Crystallography*, vol. IV, Eds. J. A. Ibers and W. C. Hamilton, Kynoch, Birmingham, 1974, pp. 79, 80 and 88.
26 N. Walker and S. Stuart, *Acta Crystallogr., Sect. A*, 1983, **39**, 158.
27 M. Martínez Ripoll and F. H. Cano, *Program PESOS*, Instituto Rocasolano, CSIC, Madrid, 1975.
28 J. M. Stewart, *The X-ray 80 System*, Computer Science Center, University of Maryland, College Park, MD, 1985.
29 T. Roisnel and J. Rodríguez Carvajal, *WinPLOTR Program for Rietveld Refinement and Pattern Matching Analysis*, Laboratoire Léon Brillouin, CEA-CNRS, Centre d'Etudes de Saclay, France, 1999.
30 E. A. Boudreaux and L. N. Mulay, *Theory and Applications of Molecular Paramagnetism*, Wiley, New York, 1976, pp 494–495.
31 C. Cascales and C. Zaldo, *J. Solid State Chem*, in the press.
32 C. Cascales, L. Bucio, E. Gutierrez Puebla, I. Rasines and M. T. Fernandez Diaz, *Phys. Rev. B*, 1998, **57**, 5240.
33 C. Gueho, D. Giaquinta, P. Palvadeus and J. Rouxel, *J. Solid State Chem.*, 1995, **120**, 7.
34 J. A. Campa, E. Gutiérrez-Puebla, M. A. Monge, C. Ruíz-Valero, J. Mira, J. Rivas, C. Cascales and I. Rasines, *J. Solid State Chem.*, 1995, **120**, 254.
35 J. A. Campa, E. Gutiérrez-Puebla, M. A. Monge, I. Rasines and C. Ruíz Valero, *J. Solid State Chem.*, 1996, **124**, 17.
36 E. L. Muetterties and L. J. Guggenberger, *J. Am. Chem. Soc.*, 1974, **96**, 1748.
37 N. E. Brese and M. O'Keeffe, *Acta Crystallog., Sect. B*, 1991, **47**, 192.
38 C. Cascales, P. Porcher and R. Sáez Puche, *J. Phys.: Condens. Matter*, 1996, **8**, 6413.
39 C. Cascales, P. Porcher and R. Sáez Puche, *J. Alloys Compd.*, 1997, **250**, 391.
40 L. Macalik, *J. Mol. Struct.*, 1997, **404**, 213.
41 L. Macalik, P. J. Dereń, J. Hanuza, W. Strek, A. A. Demidovich and A. N. Kuzmin, *J. Mol. Struct.*, 1998, **450**, 179.
42 L. Macalik, J. Hanuza, B. Macalik, W. Ryba-Romanowski, S. Golab and A. Pietraszko, *J. Lumin.*, 1998, **79**, 9.
43 L. Makalik, J. Hanuza and A. A. Kaminskii, *J. Mol. Struct.*, 2000, **555**, 289.
44 J. Hanuza, M. Maczka and J. H. van der Maas, *J. Mol. Struct.*, 1995, **348**, 349.
45 J. Hanuza, M. Maczka and J. H. van der Maas, *J. Solid State Chem.*, 1995, **117**, 177.
46 M. Maczka, S. Kojima and J. Hanuza, *J. Phys. Chem. Solids*, 2000, **61**, 735.